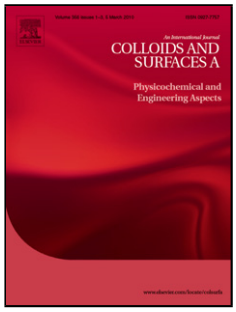

Title: Size-Dependent Electromagnetic Properties and the Related Simulations of Fe_3O_4 Nanoparticles Made by Microwave-Assisted Thermal Decomposition

Authors: Yi-Jun Liang, Fengguo Fan, Ming Ma, Jianfei Sun, Jun Chen, Yu Zhang, Ning Gu

PII: S0927-7757(17)30621-0
DOI: http://dx.doi.org/doi:10.1016/j.colsurfa.2017.06.059
Reference: COLSUA 21746

To appear in: *Colloids and Surfaces A: Physicochem. Eng. Aspects*

Received date: 23-5-2017
Revised date: 21-6-2017
Accepted date: 21-6-2017

Please cite this article as: Yi-Jun Liang, Fengguo Fan, Ming Ma, Jianfei Sun, Jun Chen, Yu Zhang, Ning Gu, Size-Dependent Electromagnetic Properties and the Related Simulations of Fe3O4 Nanoparticles Made by Microwave-Assisted Thermal Decomposition, Colloids and Surfaces A: Physicochemical and Engineering Aspectshttp://dx.doi.org/10.1016/j.colsurfa.2017.06.059

Size-Dependent Electromagnetic Properties and the Related Simulations of Fe_3O_4 Nanoparticles Made by Microwave-Assisted Thermal Decomposition

Yi-Jun Liang,[1,3,‡] Fengguo Fan,[1,3,‡] Ming Ma,[1,3] Jianfei Sun,[1,3] Jun Chen,[2] Yu Zhang,[1,3,] and Ning Gu[1,3,*]*

[1]State Key Laboratory of Bioelectronics, Jiangsu Key Laboratory for Biomaterials and Devices, School of Biological Science and Medical Engineering, Southeast University, Nanjing 210096, P. R. China.

[2]Jiangsu Cancer Hospital, the cancer Hospital of Nanjing Medical University, Nanjing 210009, P. R. China

[3]Collaborative Innovation Center of Suzhou Nano-Science and Technology, Suzhou Key Laboratory of Biomaterials and Technologies, Suzhou 215123, P. R. China

AUTHOR INFORMATION

Corresponding Authors

* E-mail: zhangyu@seu.edu.cn Fax: +86 25 83272496

* E-mail: guning@seu.edu.cn Fax: +86 25 83272460

Graphical Abstract

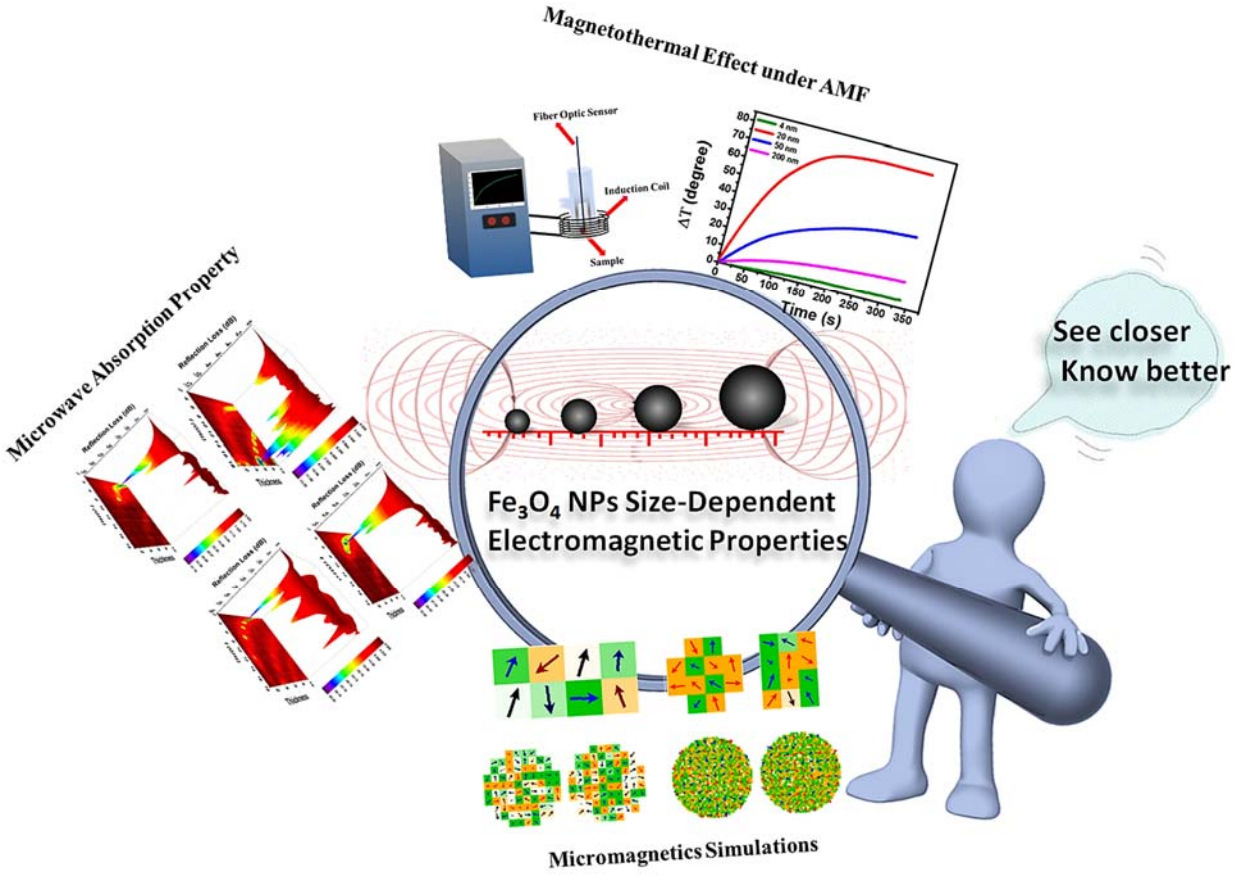

Insightfully understanding the size-dependent electromagnetic properties of magnetic NPs will be of great importance to explore their microwave applications

Graphical Abstract. To insightfully understand the size-dependent electromagnetic properties of magnetic NPs will be of great importance to explore their microwave applications.

Highlights

• High performance Fe_3O_4 NPs with different sizes were ultra-fast prepared by microwave assisted thermal decomposition approach

• The size-dependent magnetic behavior and microwave absorption performance of these Fe_3O_4 NPs was studied systematically.

• The micromagnetic simulation (OOMMF) was used to insightfully understand the size effect associated with energy variation in electromagnetic filed.

A great deal of effort has demonstrated magnetite nanoparticles (Fe_3O_4 NPs) are important subject applied in tumor hyperthermia due to their excellent magneto-thermal effect. Our previous study had ultrafast prepared 6 nm Fe_3O_4 NPs via microwave approach and found that these small size NPs are responsible for microwave energy conversion to accelerate NPs formation. Hence, we suppose that investigating the size-dependent behavior of Fe_3O_4 NPs should be beneficial for developing their electromagnetic energy conversion application for hyperthermia. In this study, Fe_3O_4 NPs with four sizes (ie. 4 nm, 20 nm, 50 nm and 200 nm) were prepared by a rapid microwave synthetic strategy. The specific absorption rate (SAR) value and reflection loss (RL) value of samples were investigated by measuring the time-dependent temperature curves in

alternating magnetic field (AMF, 390 and 780 kHz, 12A) and via vector network analyzer (VNA) range from 2-18 GHz, respectively. Results indicated that using magnetic induction hyperthermia frequency Fe_3O_4 NPs with single domain size of 20 nm possess maximum, whereas the RL value increases with the size at microwave frequency. More importantly, the frequency of maximum RL value was matched with the clinical microwave hyperthermia. We subsequently introduce the micromagnetic (OOMMF) simulation to help understanding the issue due to the fundamental importance of size effect for magnetic NPs in energy conversion. Simulation results suggested that coupling interaction and magnetic dipole-dipole interaction between magnetic NPs and electromagnetic field would be seen as synergistic effect to impact absorption behavior, and we believe that this work can provide a valuable reference for size selection of magnetic nanoparticles in clinical application of hyperthermia.

Keywords

magnetic nanoparticles, size-dependence, magnetic induction heating, microwave absorption, micromagnetics simulations

1. INTROUCTION.

In the past few years, numerous investigations have focused on utilizing high quality magnetite nanoparticles (Fe_3O_4 NPs) to solve mass practical issues, ranging from bio-medical applications to electronic device, and even for military purposes[1-3]. Currently, taking advantage from the high saturation magnetization, good stability and excellent biocompatibility of Fe_3O_4 NPs for tumor

hyperthermia have attached much concern[4-5]. The heating behavior of magnetic NPs not only can be induced by alternating magnetic field in terms of the linear response theory of Rosensweig (Brownian relaxation and Néel relaxation) or nonlinear hysteresis losses, but also arisen from magnetic NPs to absorb the electromagnetic wave and then attenuate it in the form of thermal energy via magnetic or dielectric loss, respectively[6-8].

Since the magnetic property of Fe_3O_4 NPs has been shown to have a direct impact on hyperthermia performance, and the enhanced heating efficiency can be achieved by optimizing their geometric shape, surface modification and composition, masses of synthetic method have been made and demonstrated this issue with promising[9-12]. However, apart from the issue mentioned above, the size factor was regarded as the most significant contributor for energy conversion while exposed to electromagnetic field to affect final properties and performances [13-16]. For instance, Ma and co-workers prepared Fe_3O_4 NPs by co-precipitation approach with different diameters. The results indicate that the SAR values are strongly size dependent while exposed them in an external alternating magnetic field (80 kHz, 32.5 kA/m). For small sizes samples of 7.5 and 13 nm, the main contribution as consequence of a combination of Néel and Brown processes, whereas the SAR values increase as sizes decreases from 416 to 46nm, then hysteresis loss took charge[17]. Besides, Lv et.al synthesized octahedral Fe_3O_4 NPs with sizes varying from 43 to 98 nm via thermal decomposition route, and they found that these NPs also exhibit high SAR values in accordance with size effect. As soon as the internal magnetic spins of NPs relax in phase, energy associated with transitions would immediately emitted as heat for high performance magnetic hyperthermia application[18].

In addition, Fe_3O_4 NPs also acting as an important subject for microwave absorption, which owing to their high saturation magnetization and fine impedance match feature to achieve

electromagnetic energy conversion [19-20], and there have been many well-known papers for magnetic NPs having excellent electromagnetic absorption performances and enhanced microwave heating behavior[21-23]. Our previous study took advantage of it to ultrafast synthesize monodisperse Fe_3O_4 NPs, and demonstrated that as-synthesized 6 nm NPs possess good absorption ability and great RL value of -15 dB at 2.45 GHz, which is responsible for conversion of microwave heat to accelerate nanoparticle ultrafast formation[24]. Similarly, Ding et al. reported a hydrogen-wet reduction template method in producing Fe_3O_4 nanodiscs with tunable size of 80 to 500 nm, the results also indicated that the particle size is crucial for the microwave electromagnetic and absorption properties of the as-synthesized nanodiscs [25].

These characteristics illustrated that the ideal absorbing performance caused by particle size could be well tuned via ingenious design of synthetic strategy. In fact, different absorption behavior have been often reported for a given nanoparticle size, which arising mainly from the inherent di□culties for obtaining monodisperse nanoparticles in a wide range of sizes using the same synthesis method. Moreover, due to the limited studies on the size-magnetic property relationships, so that a full understanding cannot be reached. Therefore, utilizing the feasible way to obtain different size NPs and figuring out the interrelation between size and microwave absorbing properties has become a particularly urgent need[26-28]. Microwave irradiation in general are thermal distributed uniformly and responsive to minimize thermal gradient, hence, could achieve enhanced reaction rate and leading better results. Recent studies have demonstrated this issue with promising and exciting, such as Li et.al used microwave heating for one-pot ultrafast self-assembly of autofluorescent polyphenol-based core@shell nanostructures[29], as well as the recent related works can be seen in literatures[30-33]. Herein, we developed a universal microwave-assisted thermal decomposition approach for Fe_3O_4 NPs preparation with 4 sizes (ie. 4 nm, 20 nm,

50 nm and 200 nm). Meanwhile, the Vibrating Sample Magnetometer (VSM), Alternating Magnetic Field (AMF) and Vector Network Analyzer (VNA) was used to evaluate the magnetic property, magnetic-induced heating and microwave absorption performance of NPs. Furthermore, the Object Oriented MicroMagnetic Framework (OOMMF) simulation was used to insightfully understand the microwave absorbing regular pattern on size e□ect. Taken together, these findings would provide evidences to improve the application of Fe_3O_4 NPs in magnetic hyperthermia.

2. MATERIALS AND METHODS.

2.1. Materials.

Ferric Acetylacetonate ($Fe(acac)_3$, 99.9 %), Oleic Acid (OA, 90 %) and Oleylamine (OAm, 90 %) were purchased from Sigma-Aldrich. Octadecene (ODE, 90 %) was obtained from Alfa Aesar. The Ethylene Glycol (EG, 99 %) and Isooctane (99 %) were purchased from Aladdin Industrial Corporation (China). Ethanol (95 %) and Acetone (99 %) were obtained from Sinopharm Chemical Reagent Inc. (China).

2.2. Synthesis of 4 sizes Fe_3O_4 NPs via Microwave-Assisted Thermal Decomposition Approach.

Fe_3O_4 NPs were synthesized via the single mode microwave reactor monowave 300 (Anton-Paar, Austria). Monowave 300 operates at 2.45 GHz frequency with a maximum input power of 850 W, temperature could be monitored by external infrared sensor (IR) and internal fiber-optic (FO) probe simultaneously. The unique Pyrex vessel can withstand the highest reaction temperature of 300 °C and pressure of 32 bar that is equipped to prevent from accident during reaction.

2.2.1. Synthesis of 4 nm Fe_3O_4 NPs.

Typically, 1 mmol $Fe(acac)_3$ was added into mixed solvent which consist of 10 mL OAm, 4 mL OA and 2 mL ODE in a 30mL Pyrex vial. Under microwave power (max. 850 W), mixture was firstly heated to 200 °C in a 'ASAP' procedure and kept 10 min. In succession, mixture was further heated up to 230 °C in 5 min then hold 15 min till reaction done. Subsequently, system was cooled down to 60 °C by compressed air in approximately 3 min. After 5 steps of operations, NPs washed with ethanol and acetone then dried fully in a vacuum oven.

2.2.2. Synthesis of 20 nm Fe_3O_4 NPs.

The 20 nm in size of Fe_3O_4 NPs were synthesized similarly to the synthetic process of 4 nm in size, 1 mmol $Fe(acac)_3$ was added to the Pyrex vial containing 8 mL OAm, 2 mL OA and 6 mL ODE. After sealing was done, the vial was heated to 200 °C in appropriate rate for ca. 5 min, and hold there for 10 min under microwave power (max. 850 W). The subsequent steps were following a similar procedure as above, expect for heating source was then heated up to 270 °C in 5 min then aged for 15 min until reaction done.

2.2.3. Synthesis of 50 nm Fe_3O_4 NPs.

The synthesis of 50 nm Fe_3O_4 NPs was conducted in a similar procedure as mentioned above, except for adding additional of 2 mL EG into the mixture solvent system. Under microwave power (max. 850 W), reaction was performed in totally the equivalent procedure.

2.2.4. Synthesis of 200 nm Fe_3O_4 NPs.

The larger size of Fe_3O_4 NPs can be formed in bulk OAm solvent. For a typical synthetic procedure of 200 nm in size, the mixture in 30 mL Pyrex vial was heated to 220 °C in appropriate rate for ca. 6 min and maintain this status for 10 min under microwave power (max. 850 W). The system was then heated to 300 °C and aged in total 30 min until reaction done.

2.3. Characterization of Fe_3O_4 NPs.

Transmission electron microscopy (TEM, Tokyo JEOL JEM-2100) with the addition of high-resolution (HRTEM) and selected area electron diffraction (SAED) pattern was used to identify the morphology and microstructure of microwave formed Fe_3O_4 NPs. The diameters of NPs were measured with a particle size/potential analyzer (Malvern, Zetasizer ZS90, UK). The corresponding composition of NPs was investigated by X-ray energy dispersive spectrometer (EDX, Zeiss Ultra Plus, Germany). The phase of NPs was studied by using a Powder X-ray di□raction (XRD) spectra that recorded on a Bruker X-ray di□ractometer (D8-Discover, Germany), operated at 40 mA and 40 kV. Magnetic property of the NPs was investigated in VSM (Lakeshore 7407, USA) at room temperature. Iron concentration of NPs was evaluated by classical 1,10-phenanthroline (phen) complexation spectrometry method based on the C-A (absorbance versus iron concentration) calibration curve by UV-visible spectrophotometer (Shimadzu, UV-3600, Japan).

2.4. Inductive Heating Property of NPs under AMF.

The heating experiments were accomplished in the magnetic heating system (Shuangping SPG-06-II, China) under frequency 390 and 780 kHz, 12 A respectively. 1 mL isooctane solution with iron concentration of 1 mg / mL in a thermal insulating plastic tube was placed inside the coil. The temperature was measured with a FOT series fiber optic sensor (FISO, Canada).

2.5. Electromagnetic Characterization.

The microwave electromagnetic properties for Fe_3O_4 NPs were measured by VNA (Agilent PNA N5224A) using the coaxial transmission-reflection method under the frequency range of 2-18 GHz. The samples are dispersed by homogeneously mixing with wax at the mass ratio of 7:3

and then fill as toroidal-shaped (ϕ in: 3.04 mm and ϕ out: 7.0 mm). Notably, the calibration of full two-port should be done before initially performed to remove errors. Then the permittivity and permeability can be calculated by the software which has been installed in Agilent PNA.

2.6. OOMMF Simulation.

Finite difference method was used to simulate the four sizes NPs (ie. 4 nm, 20 nm, 50 nm and 200 nm) and the same mesh of 1 nm *1 nm *1 nm was designed to be regular with shape for them, respectively. In terms of the OOMMF software description, the highest level of simulation accuracy was assigned as atomic level (10^{-10} m), hence, the currently cell size of the mesh would not affect by the precision as well as the correctness can be guaranteed [34]. Note that the frequency was inputted to be same of the microwave reactor at 2.45 GHz during the computational procedure. The Oxs Runge Kutta Evolve was defined as: Time evolver implementing several Runge-Kutta methods for integrating the Landau-Lifshitz-Gilbert. Since the smaller size superparamagnetic NPs can be seen as single domain, therefore the four sizes NPs in the alternating magnetic field were presented as a periodic sine function, and the boundary was defined according to the action time: comment {run for 20 ns total, with a stage event triggered every 1 ns.} stopping_time $1e^{-9}$.

3. RESULTS AND DISCUSSION.

3.1. Structural Characteristics.

The Fe_3O_4 NPs prepared by microwave approach with 4 different sizes were characterized by TEM, HRTEM and SAED, as well as the DLS data can be seen in Figure 1. The TEM and DLS results showed that the as synthesized Fe_3O_4 NPs with single-crystal cubic spinel structure, and the average sizes with respect to 4, 20, 50 and 200 nm, respectively (Figure 1 A1-D1 and the

insets). The HRTEM and SAED images indicated that lattice spacing of 0.281 nm and 0.289 nm could be assigned to the (220) planes of magnetite for both 4 nm and 20 nm NPs, respectively (Figure 1 A2-B2 and the insets). For 50 nm NPs, the lattice spacing of 0.462 nm and 0.249 nm could be assigned to the (111) and (311) planes (Figure 1 C2 and the inset). Also, the 200 nm in size NPs with lattice spacing of 0.463 nm was identified as the (111) plane of magnetite (Figure 1 D2 and the inset). The corresponding composition of microwave assisted thermal decomposition formed NPs was investigated by Raman spectrum in our previously report[24]. Typically, the EDX analysis further revealed the Fe and O element composition of the microwave formed samples, as shown in Figure S1 (supporting information). Besides, XRD pattern of the products at room temperature revels all the signals of NPs are highly crystalline peaks in accord with the standard crystal phase of magnetite (JCPDS No. 65-3107), (Figure S2).

3.2. Magnetic Characteristics.

It is well known the magnetic properties of NPs depend largely on particle size[35-36]. As expected, these microwave formed NPs exhibited unique size-dependent magnetic performance. The hysteresis loop measured in Figure 2A showed that the ca. 4 nm NPs are superparamagnetic due to the hysteresis loop crosses the origin and there is almost no coercivity and remnant magnetization observed. When the size increases to 20 nm, the coercivity and remnant magnetization can be clearly seen in the inset of Figure 2B and the saturation magnetization (M_s) value is 81 emu / g, which is about two times larger than the 4 nm NPs (42 emu / g). Similarly, the hysteresis loops of 50 nm and 200 nm NPs exhibited the typical ferrimagnetic hysteresis behaviors with the M_s value of 85 and 95 emu / g, respectively, which are quite close to the bulk value of Fe_3O_4 NPs (Figure 2C and D)[37].

3.3. Magnetically Induced Heating Measurements.

These 4 sizes of microwave formed products were measured in AMF to evaluate their magnetically induced heating efficiency. The specific absorption rate (SAR) value is for quantifying the heating e□ciency of the magnetic materials, in fact, it as a standard criterion is significantly related to field amplitude and frequency, M_s, particle size, etc. The value of SAR can be calculated by the following formula[38]:

$$\mathrm{SAR} = \frac{\sum C_i m_i}{m_{Fe}} \times \frac{\Delta T}{\Delta t} \qquad (1)$$

Where C_i is the specific heat of the species in solution, ΔT/Δt stands for the initial slope of T/t curve; m_i is the weight of the whole suspension and m_{Fe} means the total mass of iron. Temperature rising curves in AMF (390 and 780 kHz, 12 A) of the as-synthesized NPs are exhibited in Figure 3, as well as the calculated SAR values of NPs with uniform iron concentration of 1.0 mg /mL in isooctane solution (the specific heat capacity of isooctane is 3.23 kJ · kg^{-1} · K^{-1}) are presented in Table 1. Notably, the enhanced heating capacity which is not consistent with the saturation magnetization mentioned above, and there has no obvious heating behavior observed for the 4 nm NPs, and the 200 nm NPs, respectively. Both of them own the poor SAR values (62.5 w/g for 390 kHz and 261.9 w/g for 780 kHz). Unexpected, the 20 nm NPs possess the highest SAR value (398.4 w/g for 390 kHz and 1457.2 w/g for 780 kHz), which is 2 fold higher than 50 nm NPs (151.3 w/g for 390 kHz and 678.2 w/g for 780 kHz) under identical conditions. As previously reported, the high SAR values for 20 and 50 nm Fe_3O_4 NPs are due to comprehensive contributions from Brownian losses (friction arising from total particle oscillations), Neél losses (rotation of the magnetic moment with each field oscillation) and single domain particle hysteresis effect[39].

Obviously, these microwave formed NPs 20 nm and 50 nm NPs own the outstanding magnetic-induced heating performance will be promising for magnetic mediated hyperthermia.

3.4. Microwave Electromagnetic Properties.

In order to corroborate whether the magnetic nanomaterials possess the size-dependent microwave absorption performance or not, the corresponding electromagnetic parameters of these microwave formed Fe_3O_4 NPs were tested by VNA. Figure S3 shows the real part and imaginary part for both permittivity (ε', ε'') and permeability (μ', μ'') of the as-synthesized NPs/paraffin composite (30% mass fraction) in the frequency range of 2-18 GHz. To our best knowledge, microwave absorption properties are closely related to impedance matching, as well as the energy loss that comprised of dielectric loss and magnetic loss. Here, the ε' value is almost constant for 4 samples in the 2-14 GHz range, 4, 20 and 50 nm NPs were maintain in the value range of 5-6, whereas the 200 nm NPs kept the value around 12. In addition, the tendency of ε'' values for these four samples in general agree well with the change mentioned above, and the typical dielectric relaxation signal that value decreases with frequency increasing has not appeared[40] (Figure S3 A and B). However, different from ε' values, the ε'' value of 4 and 200 nm was much higher than 20 and 50 nm, obviously, the resonance peaks accrued not only shift across the higher frequency site (14-17 GHz) but also become stronger. The resonance behavior for 4 nm NPs may be ascribed to magnetic dipole polarization that arises from poor crystallinity, due to low aging temperature formed NPs is easy to induce the lattice defects [41]. Since the 200 nm NPs was obtained by changing the aging temperature increasing from 230 °C to 300 °C, the temperature gradient can introduce more external interface and enhance the crystallinity, so that the overall conductivity increases

with increased temperature, then leading to a simultaneous increasing in dielectric imaginary and energy loss, and more analysis and verification should be continued[42].

Interestingly, the permeability for these samples seems probably not in order, but all of the real part (μ') and imaginary part (μ'') values exhibited a sharp fall trend with increasing frequency (Figure S3C and D). Especially, the μ' value for 20 and 50 nm NPs reached the minimum at the frequency around 6-7 GHz, whereas the minimum μ' value for 4 and 200 nm NPs can be reached at the frequency of 17 and 15 GHz, respectively. Since the imaginary parts of the electromagnetic parameter imply the loss of electric and magnetic energy, hence, the increased ε'' in compared with the decreased μ'' value (-1 at 18 GHz and -0.4 at 17 GHz) for both 4 and 200 nm NPs indicated that magnetic behavior would be modulated by the dielectric behavior. It should be noted that in terms of Maxwell equations, if the magnetic field was induced by an ac electric field that would dominate the external magnetic field, and then presented the change trend of permeability inversed to that of the permittivity. Obviously, the negative permeability μ'' value was attributed to the large eddy current induced, which indicated that magnetic energy is radiated out and transferred into electric energy eventually[43] (Figure S3 C and D).

It is known that microwave magnetic loss is always in corresponding to hysteresis, eddy current loss, and resonance that composed by domain wall and natural resonance. In fact, the values of $\mu''(\mu')^{-2}f^{1}$ should be constant as frequency increases if the magnetic loss only originates from the eddy current loss, otherwise, other issues should be taken into consideration[44]. Apparently, the eddy current loss is predominantly contributing to μ'' for 4 sizes NPs with varying frequency[45], Figure S3E. Meanwhile, the similar tendency for magnetic loss tangent $tan\delta_{\mu}$ of these samples, Figure S3F. Therefore, the magnetic loss in our case is mainly caused by eddy current loss rather than domain wall resonance and magnetic hysteresis, due to magnetic hysteresis from irreversible

magnetization only takes place with strong applied field, as well as the domain wall resonance occurs usually in lower frequency (MHz)[46].

In addition, based on the measured data of the complex permittivity and permeability, the reflection loss value (RL) at a given frequency and coating thickness was calculated from the transmission line theory[47]:

$$Z_{in} = Z_0\sqrt{\frac{\mu_r}{\varepsilon_r}}\tan h\left(j\frac{2\pi fd}{c}\sqrt{\mu_r\varepsilon_r}\right) \quad (2)$$

$$C_0 = \mu"(\mu')f^{-1} = 2\pi\mu_0 d \times 2\sigma \quad (3)$$

$$\text{RL (dB)} = 20\log|(Z_{in} - Z_0) \div (Z_{in} + Z_0)| \quad (4)$$

Where Z_{in} as the input impedance of the sample and Z_0 is treated as the impedance of air, as well as f is the matching frequency, c is the velocity of the electromagnetic wave in free space while d is the thickness of the sample. As shown in Figure 4, all the RL curves reached minimum values when the coating thickness and frequency satisfied the matching relationship. Notably, a considerable RL less than -10 dB covering the frequency range of 2-4 GHz is regarded as the suitable microwave hyperthermia medium. In fact, the 4 nm NPs exhibit the maximum RL value of -12.8 dB at 17.5 GHz (thickness of 6 mm), and the bandwidth less than -10 dB covering the 16.4-18 GHz range (Figure 4A). Meanwhile, the maximum RL value -33.7 dB occurred at 4.6 GHz on the same thickness, and the bandwidth less than -10 dB covering the 2.3-7.7GHz range was observed for 20 nm NPs, Figure 4B. However, the 50 nm NPs own the maximum RL of -37 dB at 2.68 GHz, and the RL value less than -10 dB was covered the range from 2 to 7.6 GHz. Among which, the 200 nm NPs possess the highest RL value of -40.2 dB in 6 mm thicknesses (2.96 GHz), and the absorption range less than -10 dB was located at the range between 2 to 8.9 GHz, Figure 4C and D. As a result, RL values raised with increasing size from 4 to 200 nm, moreover, based on the microwave absorption features, we believe that the larger size NPs (ie. 50

and 200 nm) are more suitable as energy conversion medium to meet the requirements of microwave therapy.

3.5. Micromagnetic (OOMMF) Simulation.

Since the size-dependent microwave absorption and electromagnetic waves attenuation behavior was confirmed by Fe_3O_4 NPs to achieve energy conversion, hence, it is necessary by virtue of OOMMF simulation for providing theoretical basis to figure out the intrinsic mechanism of relevant energy variation with different size. We firstly simulated the circumstance which only in presence of single particle under the electromagnetic field, and the corresponding arrangements of the magnetic moments in one period sine wave (0 s~3.04 e^{-10} s) for these 4 different sizes samples were exhibited in Figure 5. Though subjects were set in the same sphere-like morphology to suppress interference for easier comparison, the magnetization status in given fields were significantly different at the same time. While at original time (0s) without applied magnetic field, the magnetic moments were disordered for all NPs. As time goes by, the arrangement of magnetic moments for 4nm, 20 nm and 50 nm NPs keep rotating different degrees with interaction time, whereas for the 200 nm in size NPs exhibited vortex-like phenomenon. The behavior was matched with the trend of size effect due to magnetite NPs become a single domain when the size is smaller than 50 nm, the magnetization status is randomized by thermal energy to present superparamagnetic. As the size gained to be multi-domain, where coercivity could be maximized in behavior of ferrimagnetic or ferromagnetic[48]. In addition, we also investigated the status while there were two particles in electromagnetic field with same conditions for further explore the effect of the dipole interaction between magnetic nanoparticles on microwave absorption properties under electromagnetic field, the variation in trend for 4nm, 20 nm were similar at the same point

under microwave magnetic field. Whereas for 50 nm NPs was found to be vortex-like, and different from both, the magnetic moments were disordered for the 200 nm sample, which means that the interaction between particles affects the rotation of magnetic moment (Figure S4).

Taking into consideration that the total free energy of the system mainly composed by magnetostatic energy, anisotropy energy, exchange and Zeeman energy, hence, not a single one can be omitted due to it can reflect the stabilized state of magnetic NPs magnetization and their dynamic process under the electromagnetic field. The value of free energy can be deduced in terms of the Landau-Lifshitz-Gilbert formula[49-50]:

$$\frac{\mathrm{dM}}{\mathrm{dt}} = -|\gamma| M \times H_{eff} + \frac{\alpha}{M_s}\left(M \times \frac{\mathrm{dM}}{\mathrm{dt}}\right) \qquad (5)$$

Where M is the magnetization, H_{eff} is the effective field and α means the damping constant, as well as γ is the Gilbert gyromagnetic ratio. Generally speaking, the magnetostatic energy is making responsible for the magnetic domain to be generated within the magnetic NPs. In Figure 6A, the magnetostatic energy exhibited size-dependence. For 200 nm in size NPs, the value decreases sharply to reach a minimum then surrounding in periodic change. In comparison, the 50 nm NPs presented periodical trend change with time, whereas there has no obvious changing tendency for 4 and 20 nm particle due to the multi-domain structure and its movement is chaos for larger size NPs, which would consume far more energy for domain walls keep moving while they become pinned at grain boundaries through a sample[51]. The tendency of anisotropy energy (magneto-crystalline anisotropy) was similar for 200 nm particle as plotted in Figure 6B, except the value was increased in the short beginning and then maintain the cycle fluctuations change, however, the value decreases with the size decreeing for 50 nm, 20 nm and 4 nm particle, respectively. The variation may in correspondence with the status of spin-orbit coupling, which could determine the direction of magnetization for each magnetic domain in electromagnetic field [52].

From the comparison in exchange energy, the value for both 50 and 200 nm decreases to reach a minimum then became a constant, instead, the variation tendency for 4 and 20 nm are very trivial. The situation indicated that in order to hinder the spin rotation, the parallel orientation of the atomic magnetic moment inside the magnetic domain should overcome greater resistance for large size NPs[53], Figure 6C. Meanwhile, part of Zeeman energy change is the same as to anisotropy energy except the 200 nm NPs fluctuated in sharp distinction, which means that 200 nm Fe_3O_4 NPs show stronger magnetic coupling interaction with microwave electromagnetic field than the others[54], Figure 6D.

Turning the case while concerning the interaction between magnetic NPs under the identical conditions, apparently, the value of free energy for whole system increased significantly in comparison to the case of single particle in electromagnetic field, which was ascribed to the magnetic dipole-dipole interaction between MNPs had made a positive contribution, Figure S5 A-D. The results from two models provide persuasive evidence for demonstrating the absorption properties are strongly size dependent due to the larger size particle is more sensitive to the magnetic field than the small one. More importantly, as the size increases, the coupling effect between magnetic NPs combined with the interaction of electromagnetic field will be considered as the synergistic effect to impact microwave absorption properties[55-56].

4. CONCLUSION.

In conclusion, the Fe_3O_4 NPs with different sizes were synthesized by our rapid microwave-assisted thermal decomposition approach. These microwave formed magnetic NPs exhibit interesting size-dependent magnetic behavior and microwave absorption performance. Moreover, due to the fundamental importance of size effect for magnetic NPs in energy conversion, we

introduce the micromagnetic (OOMMF) simulation to help understanding the issue. The internal connection between size and energy can be explained by Landau-Lifshitz-Gilbert equation. The critical issue for size-dependent microwave absorption performance concern energy variation, which was highly correlative with the electromagnetic field and interaction between NPs. We strongly believe that, this work would not only deepen the understanding of size dependent microwave absorption properties of magnetic NPs, but also can enrich the microwave applications.

SUPPORTING INFORMATION

The EDX analysis of microwave formed Fe_3O_4 NPs, XRD patterns of NPs with difference sizes, electromagnetic parameters and OOMMF simulation of two particles in electromagnetic field.

Author Contributions

‡These two authors (Yi-Jun Liang and Fengguo Fan) contributed equally to this work. All authors have given approval to the final version of the manuscript.

Notes

All authors declare no competing financial interest.

ACKNOWLEDGMENTS

This research was supported by the National Program on Key Basic Research Project (No. 2013CB733800), the National Natural Science Foundation of China (No. 81571806, 81271677, 81671820), and National Natural Science Foundation of China for Key Project of International Cooperation (61420106012), the Jiangsu Provincial Special Program of Medical Science (No. BL2013029), the Jiangsu Provincial Technical Innovation Fund for Scientific and Technological

Enterprises (No. SBC201310643), and a Talent 333 Project in Jiangsu Province (No. BRA2015492).

REFERENCES

[1] L.H. Wu, A. Mendoza-Garcia, Q. Li, S.H. Sun. Organic phase syntheses of magnetic nanoparticles and their applications, Chem. Rev. 116 (2016) 10473-10512.

[2] D.S. Ling, T. Hyeon. Chemical design of biocompatible iron oxide nanoparticles for medical applications, Small. 9 (2013) 1450-1466.

[3] Z.Y. Wang, C.J. Liu. Preparation and application of iron oxide/graphene based composites for electrochemical energy storage and energy conversion devices: current status and perspective, Nano Energy. 11 (2015) 277-293.

[4] D. Cabrera, J. Camarero, D. Ortega, F.J. Teran, Influence of the aggregation, concentration, and viscosity on the nanomagnetism of iron oxide nanoparticle colloids for magnetic hyperthermia, J. Nanopart. Res. 17 (2015) 121.

[5] A.H. Lu, E.L. Salabas, F. Schüth, Magnetic nanoparticles: synthesis, protection, functionalization, and application, Angew. Chem. Int. Ed. 46 (2007) 1222-1244.

[6] J. Kolosnjaj-Tabi, C. Wilhelm, Magnetic nanoparticles in cancer therapy: how can thermal approaches help? Future Medicine. 12 (2017) 573-575.

[7] J.P. Fortin, C. Wilhelm, J. Servais, C. Ménager, J.C. Bacri, F. Gazeau, Size-sorted anionic iron oxide nanomagnets as colloidal mediators for magnetic hyperthermia, J. Am. Chem. Soc. 129 (2007) 2628-2635.

[8] H.L. Xu, H. Bi, R.B. Yang. Enhanced microwave absorption property of bowl-like Fe_3O_4 hollow spheres/reduced graphene oxide composites, Journal of Applied Physics. 111 (2012) 07A522.

[9] J. Xie, C.Z. Yan, Y. Zhang, N. Gu, Shape evolution of “multibranched” Mn-Zn Ferrite nanostructures with high performance: a transformation of nanocrystals into nanoclusters, Chem. Mater. 25 (2013) 3702-3709.

[10] A.B. Salunkhe, V.M. Khot, S.H. Pawar. Magnetic hyperthermia with magnetic nanoparticles: a status review, Curr. Top. Med. Chem. 14 (2014) 572-594.

[11] X.L. Liu, H.M. Fan, J.B. Yi, Y.Yang, E.S.G. Choo, J.M. Xue, D.D. Fan, J. Ding, Optimization of surface coating on Fe_3O_4 nanoparticles for high performance magnetic hyperthermia agents. J. Mater. Chem. 22 (2012) 8235-8244.

[12] J. Jang, H. Nah, J.H. Lee, S.H. Moon, M. Kim, J. Cheon, Critical Enhancements of MRI Contrast and Hyperthermic Effects by Dopant□Controlled Magnetic Nanoparticles, Angew. Chem. Int. Edit. 121 (2009) 1260-1264.

[13] M. Gonzales-Weimuller, M. Zeisberger, K.M. Krishnan, Size-dependant heating rates of iron oxide nanoparticles for magnetic fluid hyperthermia, J. Magn. Magn. Mater. 2009, 321, 1947-1950.

[14] B. Mehdaoui, A. Meffre, J. Carrey, L. Lacroix, M. Gougeon, S. Lachaize, B. Chaudret, M. Respaud, Optimal size of nanoparticles for magnetic hyperthermia: a combined theoretical and experimental study, Adv. Funct. Mater. 21 (2011) 4573-4581.

[15] K.D. Bakoglidis, K. Simeonidis, D. Sakellari, G. Stefanou, M. Angelakeriset, Size-dependent mechanisms in AC magnetic hyperthermia response of iron-oxide nanoparticles, IEEE T. Magn. 48 (2012) 1320-1323.

[16] R. Hergt, S. Dutz, M. Röder, Effects of size distribution on hysteresis losses of magnetic nanoparticles for hyperthermia, Journal of Physics: Condensed Matter, 20 (2008) 385214.

[17] M. Ma, Y. Wu, J. Zhou, Y.K. Sun, Y. Zhang, N. Gu, Size dependence of specific power absorption of Fe_3O_4 particles in AC magnetic field, J. Magn. Magn. Mater. 268 (2004) 33-39.

[18] Y. Lv, Y. Yang, J. Fang, H. Zhang, E. Peng, X. Liu, W. Xiao, J. Ding, Size dependent magnetic hyperthermia of octahedral Fe_3O_4 nanoparticles, RSC Adv. (2015) 76764-76771.

[19] G.X. Tong, Y. Liu, T.T. Cui, Y. Li, Y.T. Zhao, J.G. Guan, Tunable dielectric properties and excellent microwave absorbing properties of elliptical Fe_3O_4 nanorings, Appl. Phys. Lett. 108 (2016) 072905.

[20] G.V. Kurlyandskaya, J. Cunanan, S.M. Bhagat, J.C. Aphesteguy, S.E. Jacobo, Field-induced microwave absorption in Fe_3O_4 nanoparticles and Fe_3O_4/polyaniline composites synthesized by different methods, J. Phys. Chem. Solids. 68 (2007) 1527-1532.

[21] G.B. Sun, B.X. Dong, M.H. Cao, B.Q. Wei, C.W. Hu, Hierarchical dendrite-like magnetic materials of Fe_3O_4, γ-Fe_2O_3, and Fe with high performance of microwave absorption, Chem. Mater. 23 (2011) 1587-1593.

[22] W. Zhou, X. Hu, C. Sun, J. Yan, S. Zhou, P. Chen, Microwave absorbing properties of Fe_3O_4-

poly (3, 4□ethylenedioxythiophene) hybrids in low□frequency band, Polym. Adv. Technol. 25 (2014) 83-88.

[23] J.A. Pearce, J.R. Cook, S.Y. Emelianov, Ferrimagnetic nanoparticles enhance microwave heating for tumor hyperthermia therapy. 2010 Annual International Conference of the IEEE Engineering in Medicine and Biology, IEEE, (2010) 2751-2754.

[24] Y.J. Liang, Y. Zhang, Z.R. Guo, J. Xie, T.T. Bai, J.M. Zou, N. Gu, Ultrafast Preparation of Monodisperse Fe_3O_4 Nanoparticles by Microwave□Assisted Thermal Decomposition, Chem. Eur. J. 22 (2016) 11807-11815.

[25] Y. Yang, M. Li, Y.P. Wu, B.Y. Zong, J. Ding, Size-dependent microwave absorption properties of Fe_3O_4 nanodiscs, RSC Adv. 6 (2016) 25444-25448.

[26] A. Demortiere, P. Panissod, B.P. Pichon, G. Pourroy, D. Guillon, B. Donnio, S. Bégin-Colin, Size-dependent properties of magnetic iron oxide nanocrystals. Nanoscale. 3 (2011) 225-232.

[27] Y. Liu, T.T. Cui, T. Wu, Y. Li, G.X. Tong, Excellent microwave-absorbing properties of elliptical Fe_3O_4 nanorings made by a rapid microwave-assisted hydrothermal approach, Nanotechnology. 27 (2016) 165707.

[28] Z. Nemati, J. Alonso, L.M. Martínez, E. Garaio, J.A. Garcia, M.H. Phan, H. Srikanth, Enhanced magnetic hyperthermia in iron oxide nano-octopods: size and anisotropy effects, J. Phys. Chem. C. 120 (2016) 8370-8379.

[29] J. Fei, J. Zhao, C. Du, A. Wang, H. Zhang, L. Dai, J.B. Li, One-pot ultrafast self-assembly of autofluorescent polyphenol-based core@shell nanostructures and their selective antibacterial application, ACS nano. 8 (2014) 8529-8536.

[30] S. S. Dunna, D. R. Beckford Veraa, S. R. Benhabbourc, M. C. Parrott, Rapid microwave-assisted synthesis of sub-30nm lipid nanoparticles, Journal of Colloid and Interface Science. 488 (2017) 240-245.

[31] V. Chikan, E. J. McLaurin, Rapid Nanoparticle Synthesis by Magnetic and Microwave Heating, Nanomaterials. 6 (2016) 85-93.

[32] G. Lv, X. Xing, L. Liao, P. An, H. Yin, L Mei, Z. Li, Synthesis of birnessite with adjustable electron spin magnetic moments for the degradation of tetracycline under microwave induction, Chemical Engineering Journal, 326 (2017) 329-338.

[33] A. F. Arif, Y. Kobayashi, R. Balgis, T. Ogiet, H. Iwasaki. K. Okuyama, Rapid microwave-assisted synthesis of nitrogen-functionalized hollow carbon spheres with high monodispersity, Carbon. 107 (2016) 11-19.

[34] D.G. Porter, M.J. Donahue, R.D. McMichael, J.L. Blue, OOMMF: Public Domain Micromagnetic Software, MMM-Intermag Conference, 1998. Abstracts. The 7th Joint. IEEE (1998) 113-113.

[35] H. Iidaa, K. Takayanagia, T. Nakanishib, T. Osaka, Synthesis of Fe_3O_4 nanoparticles with various sizes and magnetic properties by controlled hydrolysis, J. Colloid. Interf. Sci. 314 (2007) 274-280.

[36] S.H. Xuan, Y.X.J. Wang, J.C. Yu, K.C.F. Leung, Tuning the grain size and particle size of superparamagnetic Fe_3O_4 microparticles, Chem. Mater. 21 (2009) 5079-5087.

[37] G.F. Goya, T.S. Berquo´; F.C. Fonseca, Static and dynamic magnetic properties of spherical magnetite nanoparticles, J. Appl. Phys. 94 (2003) 3520-3528.

[38] S. Mornet, S. Vasseur, F. Grasset, E. Duguet, Magnetic nanoparticle design for medical diagnosis and therapy, J. Mater. Chem. 14 (2004) 2161-2175.

[39] Z. Nemati, J. Alonso, L.M. Martínez, H. Khurshid, E. Garaio, J.A. Garcia, M.H. Phan, Enhanced magnetic hyperthermia in iron oxide nano-octopods: size and anisotropy effects, J. Phys. Chem. C. 120 (2016) 8370-8379.

[40] Z.Z. Wang, H. Bi, P.H. Wang, M. Wang, Z.W. Liu, L. shen, X.S. Liu, Magnetic and microwave absorption properties of self-assemblies composed of core-shell cobalt-cobalt oxide nanocrystals, Phys. Chem. Chem. Phys. 17 (2015) 3796-3801.

[41] R.C. Che, L.M. Peng, X.F. Duan, Q. Chen, X.L. Liang, Microwave absorption enhancement and complex permittivity and permeability of Fe encapsulated within carbon nanotubes, Adv. Mater. 16 (2004) 401-405.

[42] J.P. Zou, Z.Z. Wang, M.Q. Yan, H. Bi, Enhanced interfacial polarization relaxation effect on microwave absorption properties of submicron-sized hollow Fe3O4 hemispheres, J. Phys. D. Appl. Phys. 47 (2014) 275001.

[43] N.A. Buznikov, The effect of surface domain structure on low-field microwave absorption of magnetic microwires, J. Phys. D: Appl. Phys. 43 (2010) 055002.

[44] N.N. Song, Y.J. Ke, H.T. Yang, H. Zhang, X.Q. Zhang, B.G. Shen, Z.H. Cheng, Integrating giant microwave absorption with magnetic refrigeration in one multifunctional intermetallic compound of $LaFe_{11.6}Si_{1.4}C_{0.2}H_{1.7}$, Sci. Rep. 3 (2013) 2291-2295.

[45] Y.J. Chen, P. Gao, R.X. Wang, C.L. Zhu, L.J. Wang, M.S. Cao, H.B. Jin, Porous Fe_3O_4/SnO_2 core/shell nanorods: synthesis and electromagnetic properties, J. Phys. Chem. C. 113 (2009) 10061-10064.

[46] J. Wei, J.H. Liu, S.M. Li, Electromagnetic and microwave absorption properties of Fe_3O_4 magnetic films plated on hollow glass spheres, J. Magn. Magn. Mater. 312 (2007) 414-417.

[47] J.W. Liu, R.C. Che, H.J. Chen, F. Zhang, F. Xia, Q.S. Wu, M. Wang, Microwave absorption enhancement of multifunctional composite microspheres with spinel Fe_3O_4 cores and anatase TiO_2 shells, Small. 8 (2012) 1214-1221.

[48] D.S. Ling, N. Lee, T. Hyeon, Chemical synthesis and assembly of uniformly sized iron oxide nanoparticles for medical applications, Acc. Chem. Res. 48 (2015) 1276-1285.

[49] T.L. Gilbert, A Lagrangian formulation of the gyromagnetic equation of the magnetization field, Phys. Rev. 100 (1955) 1243.

[50] L. Landau, E. Lifshitz, On the theory of the dispersion of magnetic permeability in ferromagnetic bodies. Physick. Z. Sowjetunion, 8 (1935) 153-169.

[51] O. Tchernyshyov, G.W. Chern, Fractional vortices and composite domain walls in flat nanomagnets, Phys. Rev. Lett. 95 (2005) 192704.

[52] G.H.O. Daalderop, P.J. Kelly, M.F.H. Schuurmans, Magnetocrystalline anisotropy and orbital moments in transition-metal compounds, Phys. Rev. B. 44 (1991) 12054-12057.

[53] R.P. Cowburn, D.K. Koltsov, A.O. Adeyeye, M.E. Welland, D.M. Tricker, Single-domain circular nanomagnets, Phys. Rev. Lett. 83 (1999) 1042-1045.

[54] K. Nishioka, C. Hou, H. Fujiwara, R.D. Metzger, Grain size effect on ferro antiferromagnetic coupling of NiFe/FeMn systems, J. Appl. Phys. 80 (1996) 4528-4533.

[55] G.T. Landi, Role of dipolar interaction in magnetic hyperthermia, Phys. Rev. B. 89 (2014) 014403.

[56] D.F Coral, P. Mendoza Zélis, M. Marciello, H. Khurshid, E. Garaio, J.A. Garcia, M.H. Phan, H.Srikanth, Effect of nanoclustering and dipolar interactions in heat generation for magnetic hyperthermia, Langmuir. 32 (2016) 1201-1213.

Figure captions.

Figure 1. TEM images, HRTEM images and corresponding SAED patterns, as well as the DLS measurement of microwave formed Fe_3O_4 NPs with difference sizes: (A) 4 nm, (B) 20 nm, (C) 50 nm and (D) 200 nm, respectively, scale bar 5 nm.

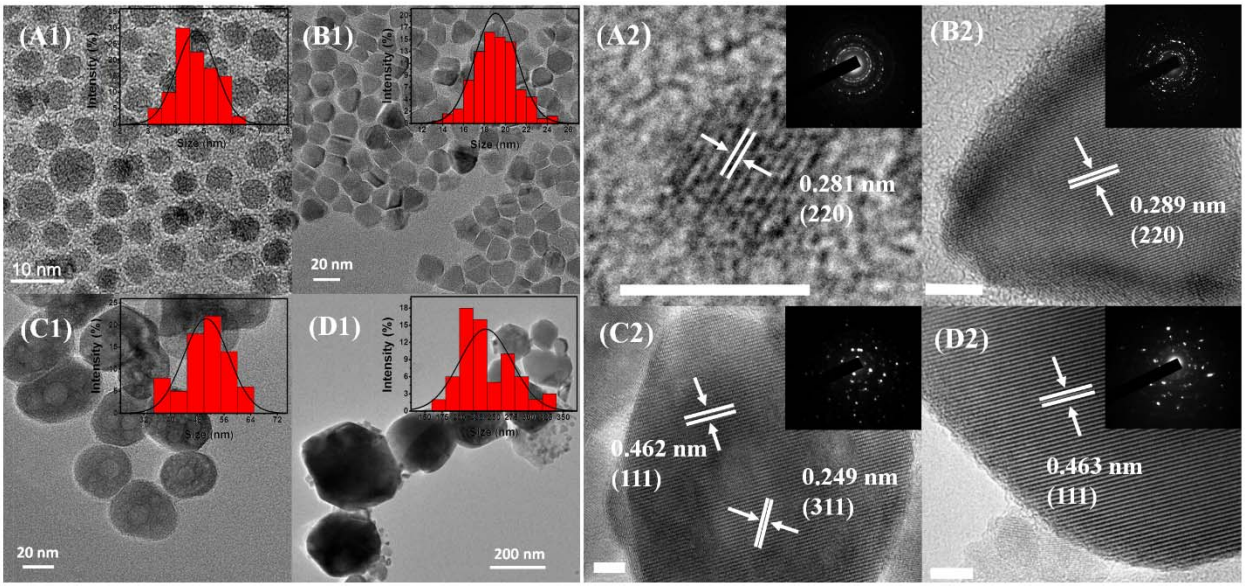

Figure 2. Field-dependent hysteresis loops (M–H) at room temperature of microwave formed Fe_3O_4 NPs with difference sizes: (A) 4 nm, (B) 20 nm, (C) 50 nm and (D) 200 nm.

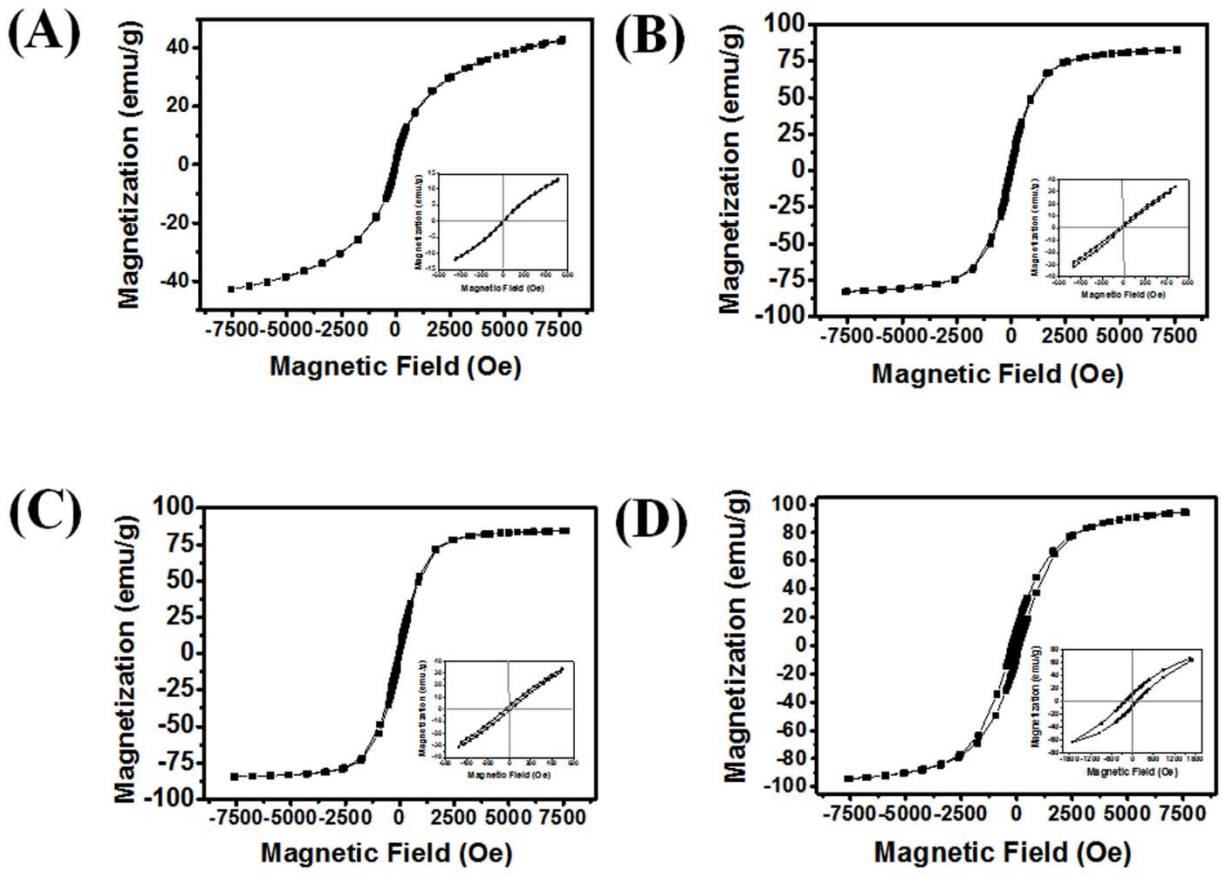

Figure 3. Experimental equipment of magnetically induced heating measurement (A), Time-dependent temperature curves of 4 sizes Fe_3O_4 NPs in isooctane (1mg/mL) under AMF with frequency of 390 kHz (B) and 780 kHz (C), and both the current are 12 A.

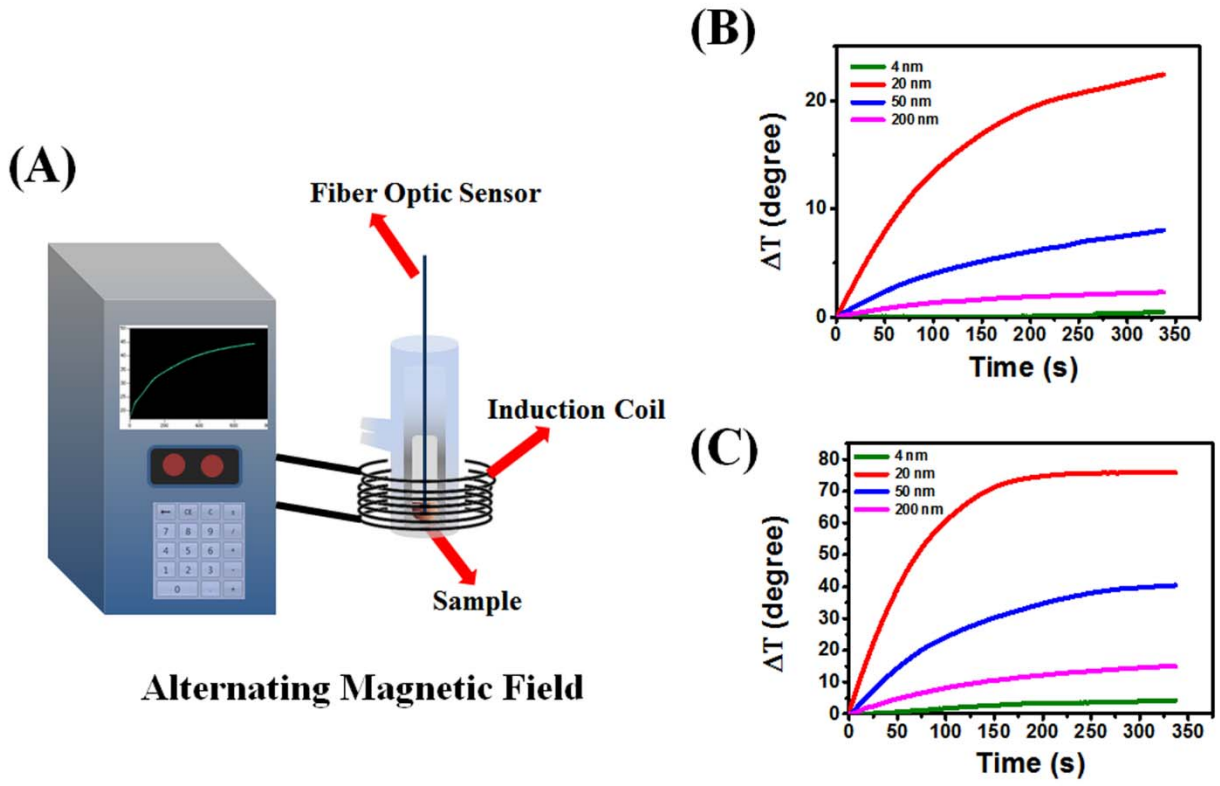

Figure 4. Frequency and thickness dependence of refection loss (RL) for (A)4 nm, (B) 20 nm, (C) 50 nm and (D) 200 nm Fe_3O_4 NPs in wax composite with different thickness, respectively.

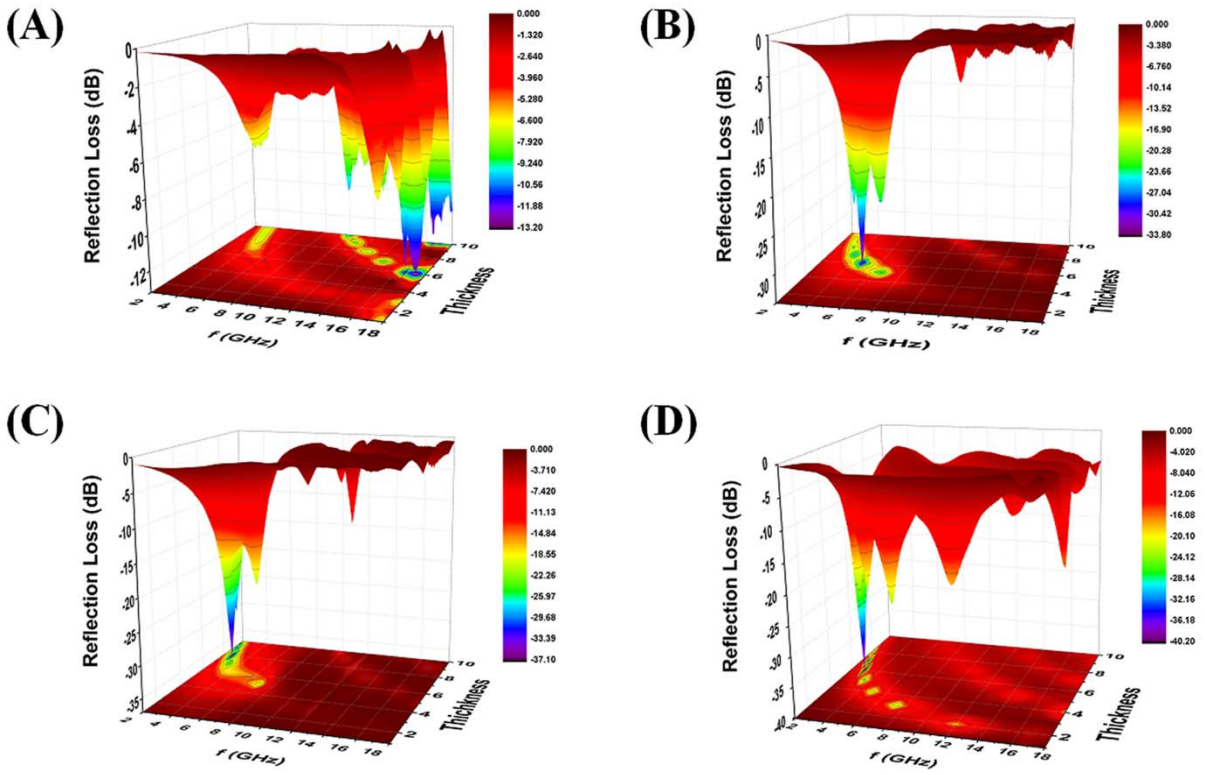

Figure 5. Corresponding OOMMF simulation on top view of magnetization status of single particle in a certain cycle (A) 4 nm, (B)20 nm (C) 50 nm and (D) 200 nm, respectively.

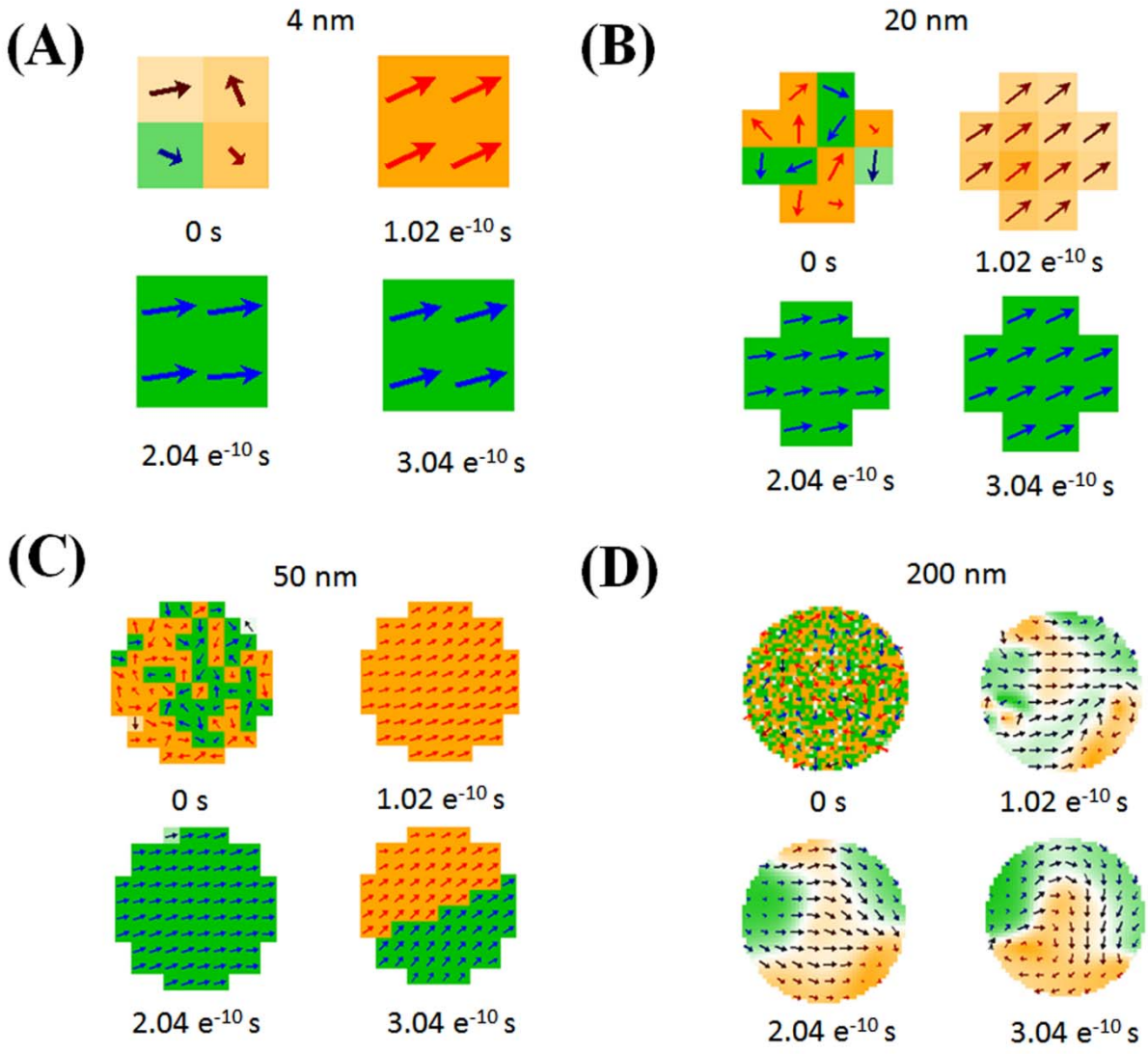

Figure 6. OOMMF simulation of Free energy dependence on time of single particle with 4 sizes for (A) magnetostatic energy, (B) anisotropy energy, (C) exchange and (D) Zeeman energy, respectively.

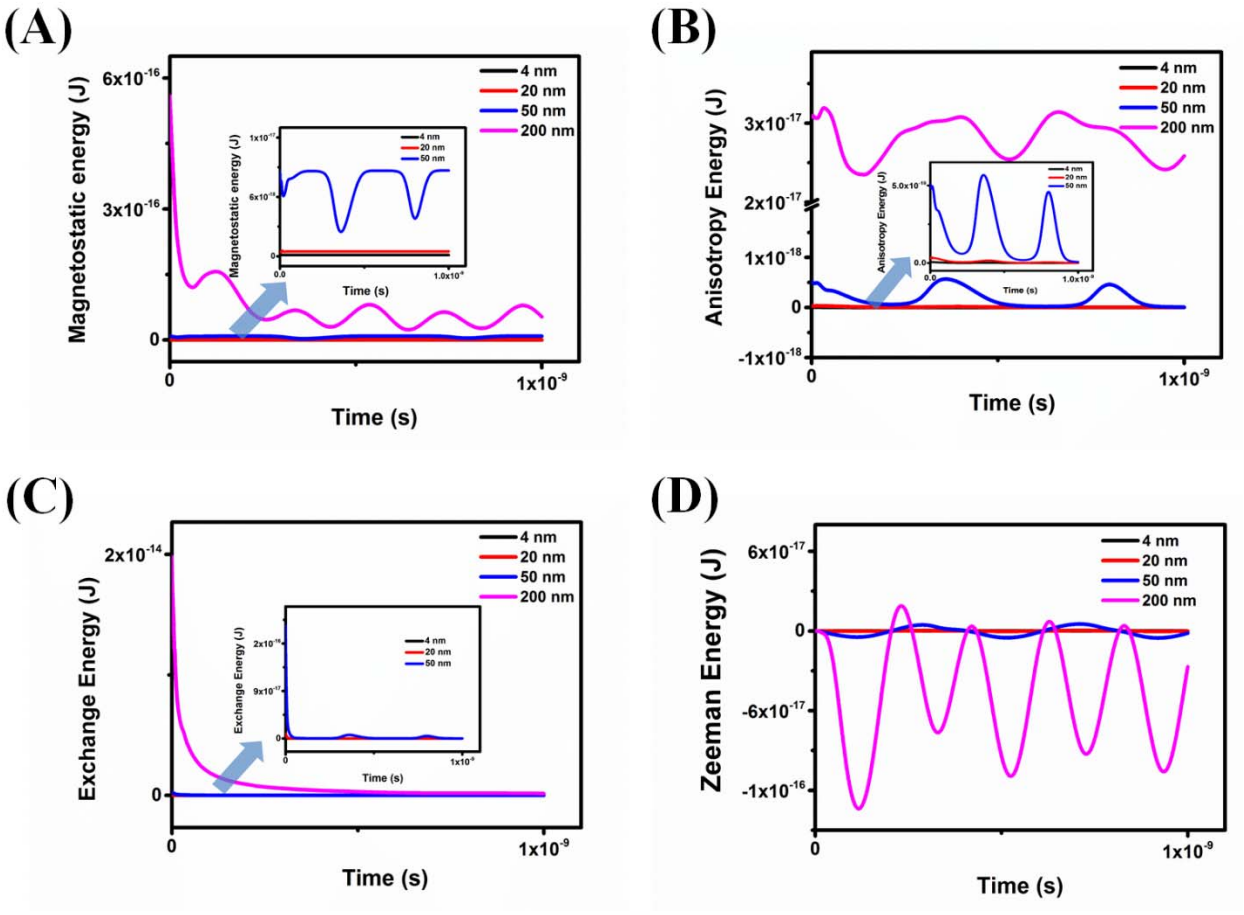

Table 1. The Calculated SAR Values, M_s and size of microwave formed Fe_3O_4 NPs.

Size (nm)	4		20		50		200	
Frequency (kHz)	390	780	390	780	390	780	390	780
Calculated SAR (w / g)	33.6	62.7	398.4	1457.2	151.3	678.2	62.5	261.9
M_s (emu / g)	42		81		85		95	